Inorganic Chemistry

Article

pubs.acs.org/IC

From Hydrated $Ni_3(OH)_2(C_8H_4O_4)_2(H_2O)_4$ to Anhydrous $Ni_2(OH)_2(C_8H_4O_4)$: Impact of Structural Transformations on Magnetic Properties

Adel Mesbah,*[,†,‡] Pierre Rabu,[§,⊥] Romain Sibille,[†] Sébastien Lebègue,[∥] Thomas Mazet,[†] Bernard Malaman,[†] and Michel François[†]

[†]Institut Jean Lamour, UMR 7198 CNRS, Université de Lorraine, BP 70239, rue du Jardin Botanique, 54506 Vandoeuvre lès Nancy, France

[∥]Laboratoire de Cristallographie, Résonance Magnétique, et Modélisations CRM2 (UMR UHP-CNRS 7036), Faculté des Sciences et Techniques, Université de Lorraine, B.P. 70239, Boulevard des Aiguillettes, 54506 Vandoeuvre-lès-Nancy Cedex, France

[§]Institut de Physique et Chimie des Matériaux de Strasbourg and NIE and Département de Chimie des Matériaux Inorganiques, UMR 7504 CNRS, Université de Strasbourg, 23 rue du Loess, B.P. 43, F-67034 Strasbourg Cedex 2, France

[⊥]Fondation icFRC, International Center for Frontier Research in Chemistry, 8 allée Gaspard Monge, F-67000, Strasbourg, France

Supporting Information

ABSTRACT: Dehydration of the hybrid compound $[Ni_3(OH)_2(tp)_2(H_2O)_4]$ (**1**) upon heating led to the sequential removal of coordinated water molecules to give $[Ni_3(OH)_2(tp)_2(H_2O)_2]$ (**2**) at T_1 = 433 K and thereafter anhydrous $[Ni_2(OH)_2(tp)]$ (**3**) at T_2 = 483 K. These two successive structural transformations were thoroughly characterized by powder X-ray diffraction assisted by density functional theory calculations. The crystal structures of the two new compounds **2** and **3** were determined. It was shown that at T_1 (433 K) the infinite nickel oxide chains built of the repeating structural unit $[Ni_3(\mu_3\text{-}OH)_2]^{4+}$ in **1** collapse and lead to infinite porous layers, forming compound **2**. The second transformation at T_2 (483 K) gave the expected anhydrous compound **3**, which is isostructural with $Co_2(OH)_2(tp)$. These irreversible transitions directly affect the magnetic behavior of each phase. Hence, **1** was found to be antiferromagnetic at T_N = 4.11 K, with metamagnetic behavior with a threshold field H_c of ca. 0.6 T. Compound **2** exhibits canted antiferromagnetism below T_N = 3.19 K, and **3** is ferromagnetic below T_C = 4.5 K.

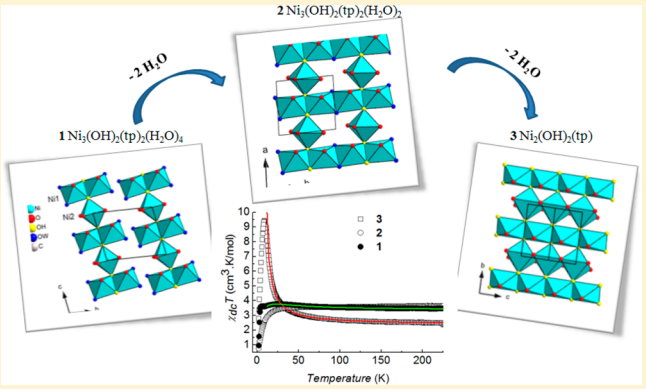

1. INTRODUCTION

Hybrid compounds composed of the association of a transition metal with carboxylates belong to a rich family of compounds known as metal−organic frameworks (MOFs). For a long time, a tremendous amount of work has focused on their crystal chemistry and potential industrial applications. They have many applications in different fields such as gas storage and separation,[1−5] drug delivery,[6] catalysis,[7,8] sensing,[9] nonlinear optics,[10] luminescence,[11] metal protection against aqueous corrosion,[12−15] and cryogenic magnetorefrigeration.[16] Moreover, they allow for the possibility of an exciting multifunctionality resulting from either the juxtaposition or the synergistic interplay between the intrinsic characteristics of each component, e.g., multiferroicity.[17,18]

Exploration of the structural properties of these materials showed that heating of compounds having a porous character up to moderate temperatures (almost always less than 473 K) was followed by the release of solvent molecules (water or other species) embedded in the micropores of the structure.[19−24] Thereafter, the adsorption performance of the evacuated "empty" compounds was measured. In those cases, the induced structural modifications correspond mainly to a change in the unit cell parameters (shift of the Bragg positions) without significant changes in the general topology of the structure. The most well-known example is the compound $Cr^{III}(OH)(O_2CC_6H_4CO_2)\cdot 0.75HO_2CC_6H_4CO_2H$, for which dehydration caused an increase of the unit cell volume by about 32%.[25] The sorption−desorption behavior was found to be reversible because of preservation of the compound's crystallinity even after evacuation of the intercalated species. This phenomenon was termed "breathing" by Férey and Serre.[26] Hence, in this example, desorption of the intercalated molecules does not directly affect the crystallographic integrity

Received: August 28, 2013
Published: January 8, 2014

   dx.doi.org/10.1021/ic402106v | Inorg. Chem. 2014, 53, 872−881

of the compounds. On the other hand, if the evacuated molecules are coordinated to the metal (first neighbors), thermal desorption usually causes amorphization or even decomposition of the compound. We can cite the example of $Ni_3(OH)_2(1,4\text{-}CDC)_2(H_2O)_4{\cdot}4H_2O$ (CDC = cyclohexanedicarboxylate), where heating directly caused amorphization of the compound around 150 °C.[27] In other cases, dehydration by heating was evidenced only by the decrease of the metal coordination number, without the occurrence of any other structural rearrangements.[28] Importantly, few MOFs showed evolution of the coordination sphere of the metal ions with a change in their dimensionality[29] and formation of anhydrous compounds.

Modification of the structural properties of these kinds of materials allowed for many applications in terms of sorption properties. Moreover, the crystallographic changes induced by thermal treatment may allow for tuning of their physical properties. In this respect, the magnetic properties are expected to be significantly influenced by variation of the distances and angles along the exchange pathway between adjacent magnetic centers. There are a few examples concerning modification of the magnetic properties with dehydration,[19,21,24] and in all cases, dehydrated water molecules were solvated and not coordinated to the metal.

In this paper, we have studied evolution of the magnetic properties as a function of the temperature of a selected MOF containing only water molecules coordinated to the metal. Therefore, a nickel hybrid compound appeared to be an ideal candidate. Indeed, most of the nickel carboxylates so far reported in the literature[30] contain water in their coordination sphere, except the cases of $Ni_5(OH)_6(C_6H_8O_4)_2$ and $Ni_5(OH)_6(C_8H_{12}O_4)_2$.[31]

Thus, compound $Ni_3(OH)_2(C_8H_4O_4)_2(H_2O)_4$ (**1**) was chosen not just because it only contains coordinated water molecules[32] but also because it is very difficult to directly synthesize an anhydrous nickel terephthalate, $Ni_2(OH)_2(C_8H_4O_4)$. The tetrahydrated compound was obtained by us in previous attempts to synthesize anhydrous $Ni_2(OH)_2(tp)$ (tp = $C_8H_4O_4^{2-}$), in order to complete the isostructural family $M_2(OH)_2tp$, where M = Co,[33] Fe and Mn,[34] Cu,[35] V,[36] and a Co−Fe solid solution.[37,38] The many attempts at direct synthesis of $Ni_2(OH)_2tp$ were not successful. Other attempts involving hydrazine as a structuring agent were performed and led to formation of the unexpected new compound $Ni(C_8H_4O_4)(C_4H_{10}N_2)$.[39]

In this paper, we report the successful preparation of anhydrous $Ni_2(OH)_2tp$ obtained through a two-step mechanism. Dehydration of **1** was carried out by heating at moderate temperatures (from room temperature to 483 K). Structural changes were evidenced by in situ powder X-ray diffraction. Dehydration led to two well-defined modifications corresponding to the formation of $[Ni_3(OH)_2(tp)_2(H_2O)_2]$ (**2**) and $Ni_2(OH)_2tp$ (**3**). Moreover, evolution of the structure induces important modification of their magnetic properties.

2. EXPERIMENTAL SECTION

2.1. Synthesis. A green powder of the aqua nickel hydroxyterephthalate $[Ni_3(OH)_2(tp)_2(H_2O)_4]$ (**1**) was synthesized hydrothermally according to a literature procedure.[32] The reactants $Ni(NO_3)_2{\cdot}6H_2O$ (Aldrich, 98%) and $Na_2C_8H_4O_4$ (Aldrich, 98%) were used as received. An aqueous solution was prepared by mixing $Ni(NO_3)_2{\cdot}6H_2O$ (1.679 g, 5.7 mmol) and $C_6H_4(CO_2Na)_2$ (1.821 g, 8.7 mmol) in a molar ratio of 3:2. The pH of the solution was adjusted to 8 by the dropwise addition of NaOH (0.1 M). The mixture was homogenized and poured into a 15-mL Teflon-walled acid digestion bomb and then heated for 72 h at 423 K. The reaction product was collected by centrifugation, washed twice with a mixture of distilled water/ethanol (1:1), and then dried overnight in air at room temperature.

2.2. IR Spectroscopy and Thermogravimetric Analysis (TGA). IR spectra were recorded by means of a Spectrum One Fourier transform infrared (FT-IR) spectrometer (Perking-Elmer Instruments) in the ATR mode using a Universal Sampling Accessory. TGA measurements were performed with a SETARAM TG/ATD 92-16.18 instrument in the range of 298−873 K under air, with a heating rate of 1 $K{\cdot}min^{-1}$.

2.3. Magnetic Measurements. Alternating-current (ac) and direct-current (dc) magnetic measurements of **1**−**3** were carried out between 2 and 300 K using the ACMS option of a Physical Properties Measurement System (Quantum Design).[40] For determination of the paramagnetic constants, χ_{dc} was measured under a field of 5000 Oe for **1**, 10000 Oe for **2**, and 1000 Oe for **3**.

2.4. Structure Determinations. In situ powder X-ray diffraction (PXRD) experiments were carried out using an XPert Pro (Panalytical, Almelo, The Netherlands) diffractometer adopting the Bragg−Brentano geometry and equipped with Cu Kα radiation, λ = 1.5418 Å. The evolution of **1** as a function of the temperature was studied from data recorded between 293 and 483 K with a step of 20 K and a counting time of 30 $min{\cdot}step^{-1}$, ranging between 16.0 and 48.0° (2θ) in a continuous scan mode [steps of 0.0167° (2θ)] by using a TTK 450 high-temperature chamber (Anton Paar, Graz, Austria). Two structural transitions were observed at 433 and 483 K, respectively. The two compounds were prepared separately by heating **1** overnight under air, in an oven at 433 and 483 K, respectively. The PXRD pattern of **2** was also recorded at room temperature in the range of 5.0−60.0° (2θ) with a step of 0.0167° (2θ) for 3 h by means of the same diffractometer, whereas the PXRD pattern of **3** was measured at 100 K with synchrotron radiation (λ = 0.79988 Å) in the Debye−Scherrer mode (capillary with diameter = 0.4 mm) using the MS powder beamline of the Swiss Light Source (SLS, Switzerland).

Qualitative analysis of the PXRD patterns (Figure 1) showed two structural transitions at 433 and 483 K leading to compounds **2** and **3**,

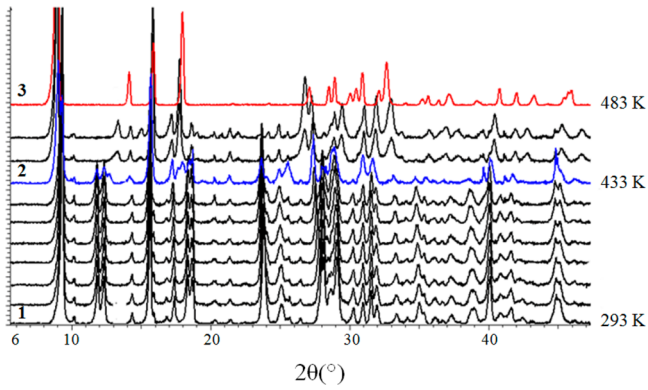

Figure 1. In situ evolution of $Ni_3(OH)_2(C_8H_4O_4)_2(H_2O)_4$ versus temperature showing two structural transitions.

respectively. Therefore, in order to solve and refine both structures, standard peak searches were performed using the program *Reflex* from Material Studio (MS) system software (*Accelrys*).[41] The unit cell parameters were determined by the indexing program *X-cell* from MS.[42] The PXRD patterns were indexed in the space group $P\bar{1}$ of the triclinic system for **2** and in the space group $C2/m$ of the monoclinic system for **3**. Refinement and structural parameters of **2** and **3** are given in Table 1.

The structure of **2** was solved ab initio in direct space using the program *FOX*.[43] This led to an initial model in agreement with the chemical formula $Ni_3(OH)_2(H_2O)_2(tp)_2$ (with the exception of the H

dx.doi.org/10.1021/ic402106v | Inorg. Chem. 2014, 53, 872−881

Table 1. Structural and Refinement Parameters for 2 and 3

	2	3
structural formula	$Ni_3(OH)_2(H_2O)_2(C_8H_4O_4)_2$	$Ni_2(OH)_2(C_8H_4O_4)$
formula mass (g)	574.34	315.46
system	triclinic	monoclinic
space group	$P\bar{1}$	$C2/m$
a (Å)	6.2784(5)	19.8413(4)
b (Å)	6.6630(3)	3.3181(1)
c (Å)	10.1465(8)	6.2682(1)
α (deg)	81.52(1)	90
β (deg)	82.59(1)	96.55(1)
γ (deg)	85.66(1)	90
volume (Å^3)	415.62(5)	409.98(1)
Z	1	2
color	green	green
D_x (g·cm^{-3})	2.295	2.297
wavelength (Å)	0.5418	0.79988
angular range (deg)	5–60	4–60
no. of obsd points	3292	5147
no. of reflns	240	229
Le Bail refinement		
R_p	0.019	0.043
R_{wp}	0.033	0.031
Rietveld refinement		
R_p	0.051	0.038
R_{wp}	0.074	0.042
R_{Bragg}	0.122	0.114
R_F	0.080	0.121
no. of soft restraints	12 distances	0
no. of profile param	11	18
no. of intensity-dependent param	16	11

atoms, which were too light to be located). The asymmetric unit of compound **2** contains two Ni sites, Ni1 in a general position and Ni2 on a symmetry center ($\bar{1}$), two tp molecules (eight C sites and four O_{carb} sites for tp, one O_w site for water molecules, and one site for OH^-). Thereafter, the H atoms were placed manually, and the structure was optimized by density functional theory (DFT) calculations. The obtained relaxed model was used to perform the final refinement with the program *FULLPROF_suite*,[44] with refinement of the tp molecules as rigid bodies. Observed, calculated, and difference patterns are shown in Figure 2, and the fractional atomic coordinates are reported in Table S1 in the Supporting Information (SI).

Refinement of the structure of compound **3** was straightforward because the unit cell parameters obtained by indexation of the PXRD pattern are similar to those of the $Co_2(OH)_2$tp structure with a = 19.8413(4) Å, b = 3.3181(1) Å, c = 6.2682(1) Å, and β = 96.55(1)°. Thus, the structure was first optimized by DFT calculations, and the final refinement was carried out using the *FULLPROF_suite* program. The structure of **3** contains a random disorder of the terephthalate (tp) molecules between the metallic layers down the a axis. This structure could be described as a mixture of two ordered models: $P2/c$ with a = 6.2595(1) Å, b = 3.3132(1) Å, c = 19.8125(3) Å, and β = 96.55(1)° with the tp molecules in a zigzag orientation down the c axis (longest) and $P\bar{1}$ (subcell) with a = 3.3128(1) Å, b = 6.2581(1) Å, c = 10.0453(2) Å, α = 96.43(1)°, β = 99.58(1)°, and γ = 90.12(1)°, where the tp molecules are parallel between the layers. The best refinement was found in the $C2/m$ space group (disordered tp molecules). The final refined atomic positions are reported in Table S2 in the SI. Metrical data of **2** and **3** are presented in Table 2, and the observed, calculated, and difference patterns are shown in Figure 2.

2.5. Neutron Diffraction Study. Powder/neutron measurements were carried out using a D1b thermal powder diffractometer located at the Institut Laue-Langevin in Grenoble, France (λ = 2.521 Å),

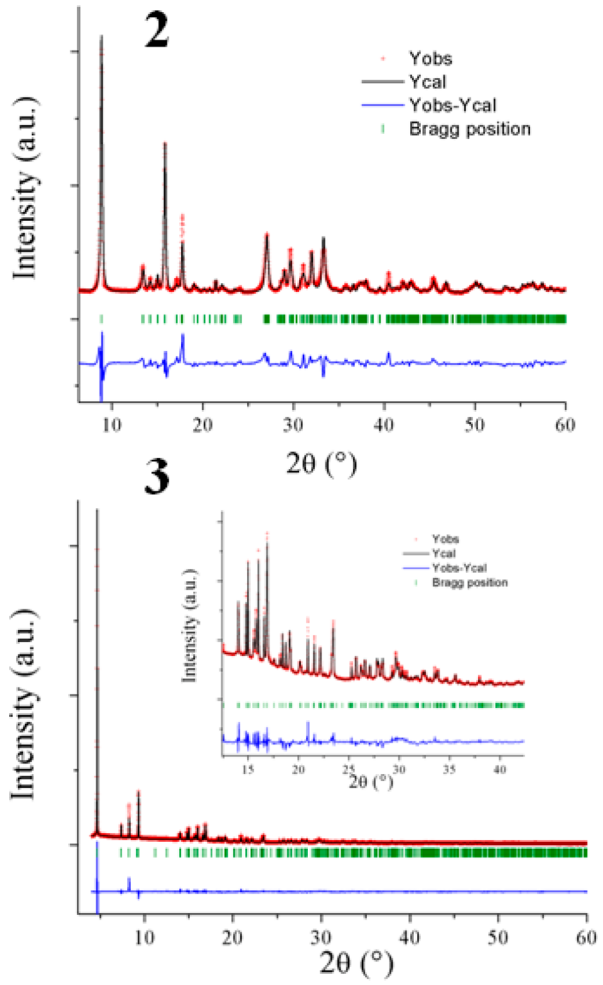

Figure 2. Observed, calculated, and difference PXRD patterns of (top) **2** and (bottom) **3** (λ = 1.0005 Å). Vertical bars indicate the Bragg positions.

equipped with a conventional "orange" helium-flow cryostat. For each sample, data sets were collected at 2.0 and 25.0 K with counting times of 2 h for each temperature; at 2.0 K, only compound **1** showed supplementary peaks corresponding to its antiferromagnetic ordering. Thus, the pattern recorded at 25.0 K (nuclear component) was refined to establish the scale factor, lattice parameters, and instrument profile function. Then, these parameters were fixed during refinement of the difference pattern between 1.6 and 25.0 K, which corresponds only to the magnetic contribution. Refinement of the neutron pattern recorded at 25.0 K led to the following unit cell parameters (R = 0.14): a = 10.207 Å, b = 7.983 Å, c = 6.321 Å, α = 97.97°, β = 97.13°, and γ = 110.07°. At 1.4 K, the new peaks corresponding to the magnetic structure were indexed by doubling a and b cell parameters. Two consistent solutions were proposed: the first with magnetic moments aligned in the ac plane with values of 1.7(4) and 1.3(5) μ_B for Ni1 and Ni2, respectively, and the second with moments aligned in the bc plane with 1.5(4) and 1.7(5) μ_B for Ni1 and Ni2, respectively. In both cases, the magnetic structure consists of ferrimagnetic chains coupled antiferromagnetically down the b axis and also through the a axis. Thus, the atoms Ni1 forming the dimers are coupled ferromagnetically and noncollinear antiferromagnetically with each adjacent Ni2. On the basis of the neutron diffraction data alone, it is not possible to determine which configuration is correct.

2.6. Computational Details. To access which configuration is the most favorable, DFT calculations[45,46] have been performed with the Vienna Ab initio Simulation Package,[47,48] implementing the projector augmented wave method.[49] Two different exchange-correlation potentials were tested, namely, the generalized gradient approximation

dx.doi.org/10.1021/ic402106v | Inorg. Chem. 2014, 53, 872–881

Table 2. Selected Bond Lengths (Å) and Angles (deg) for 2 and 3

Phase 2						
Ni1	O2	2.024(5)	O2	Ni1	O4	177.3(3)
$Ni(OH)_2O_2(H_2O)_2$	O4	1.995(5)	OH	Ni1	Ow	172.9(4)
	OH	2.077(8)	O_w	Ni1	O4	93.9(8)
	OH	2.068(6)	OH	Ni1	O4	91.7(4)
	O_w	2.175(10)	O_w	Ni1	O4	88.3(8)
	O_w	2.189(15)	O2	Ni1	O_w	89.0(8)
Ni2	O1	2 × 2.187(3)	O1	Ni2	O1	180.00
$Ni2(OH)_2O_4$	O3	2 × 2.051(3)	OH	Ni2	OH	180.00
	OH	2 × 1.987(3)	O3	Ni2	O3	180.00
			O1	Ni2	OH	90.9(3)
			OH	Ni2	O3	92.2(3)
			O1	Ni2	O3	91.12(12)
Phase 3						
Ni1	O2	2 × 2.100(4)	O2	Ni1	O2	180.0
$Ni(OH)_4O_2$	OH	4 × 2.055(4)	OH	Ni1	OH	180.0
			OH	Ni1	O2	92.7(2)
			OH	Ni1	O2	87.3(2)
Ni2	OH	2 × 2.014(7)	OH	Ni2	OH	180.0
$Ni(OH)_2O_4$	O3	4 × 2.184(2)	O1	Ni2	OH	92.2(2)
			O1	Ni2	O1	180.0
			O1	Ni2	OH	87.8(2)

(GGA) of Perdew–Burke–Ernzerhof[50] (PBE) and the GGA–PBE+U method,[51,52] with the U and J parameters aimed at emphasizing the strongly correlated nature of the d electrons of nickel. Because the results obtained with these two methods are very close to each other, we present only the results obtained with the parameter-free GGA–PBE method. The cell parameters and positions of the atoms were fixed at the values obtained experimentally, except for the H atoms, which were relaxed to their equilibrium positions in a preliminary calculation. Noncollinear ordering of the magnetic moments and spin–orbit coupling were switched on in our calculations. Also, we found that numerical convergence is reached in our calculations for a plane-wave cutoff of 400 eV and a k-point mesh in the Brillouin zone of 1 × 1 × 8.

From our calculations, the configuration with the magnetic moments in the ac plane is found to be more favorable (i.e., has a lower total energy) than the configuration with the magnetic moments in the bc plane. A projection of the magnetic structure is viewed in Figure S1 in the SI. The atomic positions and magnetic structure are reported in Table S2 in the SI.

3. RESULTS AND DISCUSSION

3.1. TGA and IR Spectroscopy. The TGA curves of **1**–**3** are shown in Figure 3. For **1**, the weight loss caused by water departure occurs in a two-step process at 423 and 523 K, respectively. Each step corresponds to a 5.6% weight loss. This observation was confirmed by TGA of **2** up to 523 K; it corresponds to an expected weight loss of about 5.6% (two H_2O) due to the transformation of **2** into **3**. Therefore, in **3**, the water molecules were completely removed. The weight loss due to combustion of the organic component is observed between 573 and 643 K for **1**–**3**. The final product is NiO (PDF: 44–1159) in each case. The total weight losses are as follows: **1**, 62.3% obsd, 63.2% calcd; **2**, 60.1% obsd, 60.97% calcd; **3**, 58.22% obsd, 58.36% calcd.

FT-IR spectra of **2** and **3** are shown in Figure 4. They have the same main characteristics as the spectrum previously reported for **1**.[32] The stretching vibrations of OH^- and para-aromatic CH groups give bands around 3600 and 1500 cm^{-1}, respectively. The two intense bands at ca. 1575 and 1380 cm^{-1} were assigned to $\nu_{as}(-COO-)$ and $\nu_s(-COO-)$, respectively. The difference between these two bands agrees with the bridging character of the $-COO^-$ groups, with two O atoms coordinated to Ni^{II}. A comparison of the spectra allows us to verify that bands corresponding to stretching vibrations of the water molecules at 3424 and 3039 cm^{-1} are visible for **1** and **2** but not for **3**.

3.2. Structures. *3.2.1. $Ni_3(OH)_2(H_2O)_4(C_8H_4O_4)_2$.* The structure of **1** was fully described in our previous work;[32] it consists of infinite chains of $[Ni_3(OH)_2(H_2O)_4]^{4+}$ interconnected by two tp molecules $(C_8H_4O_4)^{2-}$. This kind of chain is relatively well-known among organonickel compounds and can be bonded to dicarboxylate linkers such as tdc^{2-} (thiophenedicarboxylate),[53] $chdc^{2-}$ (cyclohexanedicarboxylate),[19,27] and fum^{2-} (fumarate).[54,55] The main difference between **1** and these cited compounds is in the arrangement of the dicarboxylate anions between the nickel chains. In tdc, chdc, and fum, each metallic chain is connected to four adjacent dicarboxylates by ionocovalent bonding, forming a 3D network, whereas in **1**, each nickel chain is connected to only two adjacent dicarboxylates, leading to a 2D framework (see Figure 5 of ref 32). The 2D sheets parallel to (010) are held together through hydrogen bonding. Therefore, the existence of such weak interactions in **1** is probably the key to understanding the structural transformations described hereafter.

3.2.2. $Ni_3(OH)_2(H_2O)_2(C_8H_4O_4)_2$. The structure of **2** results from coalescence of the nickel chains in **1**. This is caused by the loss of two water molecules in each formula unit and leads to the following unit cell parameters with a = 6.2784(5) Å, b = 6.6630(3) Å, c = 10.1465(8) Å, α = 81.52(1)°, β = 82.59(1)°, and γ = 85.66(1)°. The structure consists of a 3D framework with metallic layers parallel to (001) bridged by the tp anions, as shown in two different views in Figure 5. The bond-valence function in *PLATON* provides valences of 1.89 and 1.97 for Ni1 and Ni2, respectively, in **2**. The formal oxidation states in **2** can thus be assigned as three Ni^{2+}, two $(OH)^-$, and two $(C_8H_4O_4)^{2-}$.

Compared to the structure of compound **1**, the octahedral environments of Ni1 $[Ni1(\mu_3\text{-}OH)_2(O_{carb})_2(H_2O)_2]$ and Ni2

dx.doi.org/10.1021/ic402106v | Inorg. Chem. 2014, 53, 872–881

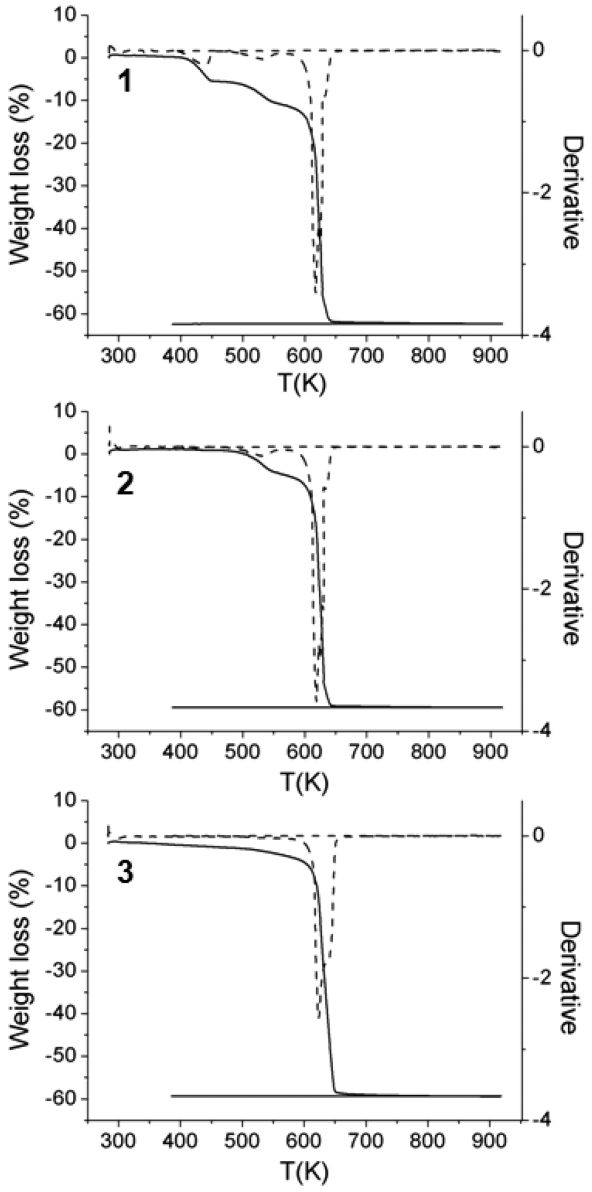

Figure 3. TGA curves of **1**−**3**.

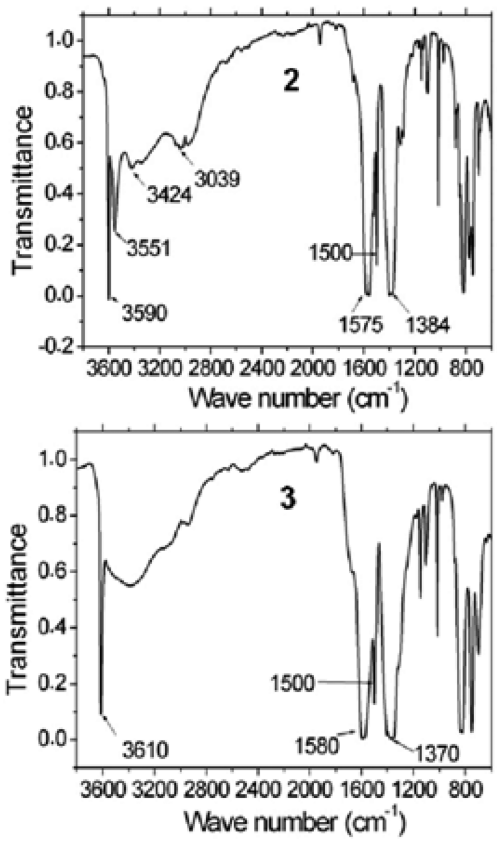

Figure 4. FT-IR spectra of **2** and **3**.

$[Ni2(\mu_3\text{-}OH)_2(O_{carb})_4]$ remain unchanged in terms of the first neighbors upon transformation from **1** to **2**. Each Ni atom is coordinated to six O atoms. The average Ni−O distances are comparable to those observed in **1**: $(Ni1-O)_{av}$ = 2.034 Å in **1** and 2.082 Å in **2**; $(Ni2-O)_{av}$ = 2.026 Å in **1** and 2.055 Å in **2**.[32]

The loss of two water molecules in the transition from **1** to **2** is also characterized by a drastic decrease of the unit cell volume by 13.3%. Indeed, parameter *b* decreases from 8.0135(1) Å in **1** to 6.6630(3) Å in **2**. This corresponds to the direction in which the 2D layers of **1** collapse. However, other parts of the structure remain unchanged. Finally, compound **2** is stable and does not allow reversible rehydration toward **1**, even after several weeks in water.

3.2.3. $Ni_2(OH)_2(C_8H_4O_4)$. Compound **3** was found to be isostructural with $Co_2(OH)_2$tp and crystallizes in space group *C*2/*m* of the monoclinic system with *a* = 19.8413(4) Å, *b* = 3.3181(1) Å, *c* = 6.2682(1) Å, and β = 96.55(1)°.[33]

The two Ni atoms are octahedrally coordinated by six O atoms. Each Ni1 is connected to four μ_3-OH and two O_{carb}. Each Ni2 is connected to two μ_3-OH and four O_{carb}. The two Ni sites are situated on a symmetry center, Ni1 (0, $^1/_2$, $^1/_2$) and Ni2 (0, 0, 0). These octahedra are connected in the (100) plane to form 2D metallic layers separated by a randomly disordered terephthalate, as observed previously with the cobalt-based compound (*C*2/*m*). The nickel octahedra are slightly distorted (see Table 2); Ni1−O distances range between 1.99 and 2.19 Å, whereas Ni2−O distances range between 1.98 and 2.05 Å. The structure charge balances with two Ni^{2+}, two OH^-, and one $(C_8H_4O_2)^{2-}$, in agreement with the bond-valence-sum calculated for Ni1 and Ni2 of 1.712 and 1.87, respectively.

The transformation at 210 °C can be described as the following:

$$\underset{\mathbf{2}}{Ni_3(OH)_2(tp)_2(H_2O)_2} \rightarrow \underset{\mathbf{3}}{Ni_2(OH)_2tp} + Ni(tp) + 2H_2O$$

The reaction balances with formation of a Ni(tp) species, which could be an analogue of the compounds $M(tp)(H_2O)_2$ (M^{II} = Mg, Mn, and Fe),[56,57] but it does not fit with the anhydrous character observed by TGA in **3**; thus, we must admit that Ni(tp) is amorphous. Several facts give proof of its existence: larger background of the PXRD pattern in **3** than those in **2** and **1** (Figure 6); larger vibrational bands of tp anions in **3** than in **2**, as shown in Figure 2; detection of an amorphous side product in **3** by transmission electron microscopy (TEM), as viewed in Figure 7.

Figure 8 depicts the transformation of the metal−oxygen network on going from **1** to **2** and from **2** to **3**. The transformation from **1** to **2** is caused by the sequential loss of two water molecules. The transformation from **2** to **3** is much

dx.doi.org/10.1021/ic402106v | *Inorg. Chem.* 2014, 53, 872−881

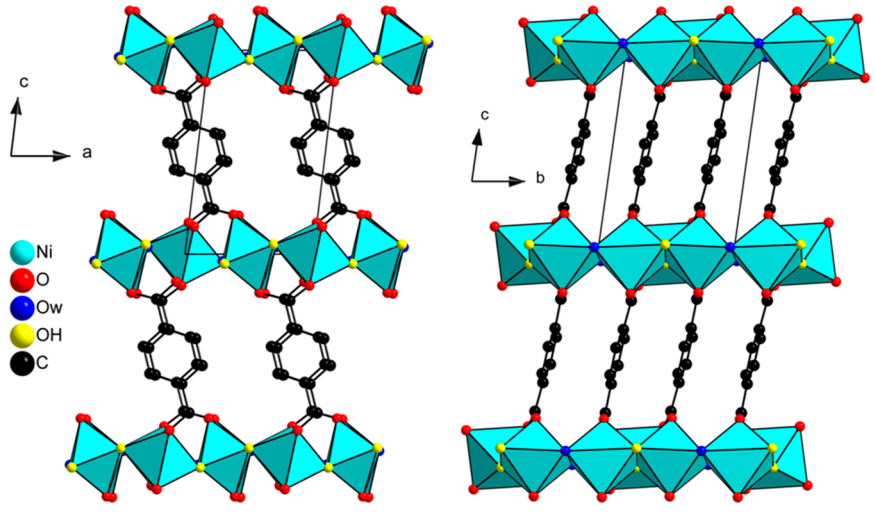

Figure 5. Structure of **2** viewed down the *b* (left) and *c* (right) axes.

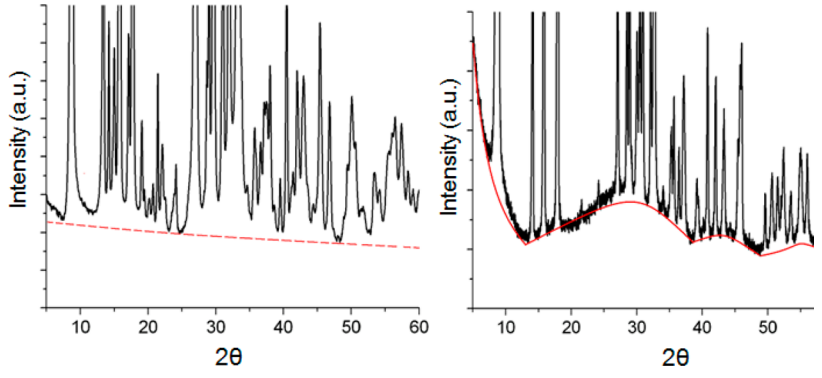

Figure 6. PXRD patterns showing the background evolution between **2** (left) and **3** (right), indicating the possible formation of an amorphous Ni(tp) phase in **3**.

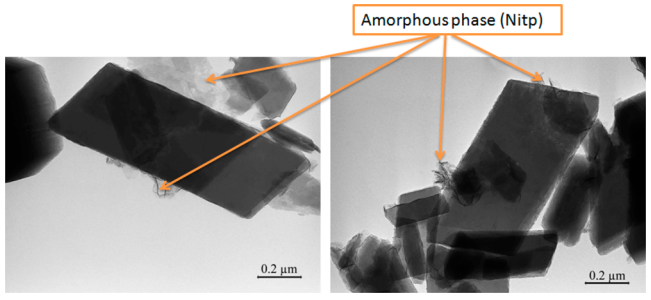

Figure 7. TEM micrographs of **3** showing the existence of side products [amorphous Ni(tp)].

more complex and involves the elimination of Ni(tp) and the remaining water molecules. In fact, it is a solid-state reaction at soft temperature realized at 483 K.

3.3. Magnetic Properties. The χT products versus temperature variation for **1**–**3** are reported in Figure 9. The three compounds exhibit linear variation of the inverse of susceptibility as a function of the temperature above 100 K. The values of the Curie constant and Weiss temperature deduced from the fit of the experimental data to the Curie–Weis law are listed in Table 3. The magnetic pathways for each compound are reported in Table 4.

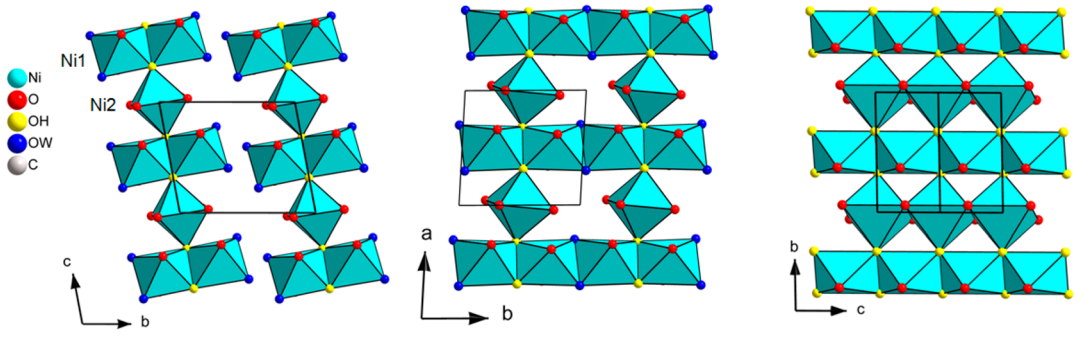

Figure 8. Transformation of the inorganic metal oxide subunits from **1** to **3** caused by the loss of water molecules.

dx.doi.org/10.1021/ic402106v | *Inorg. Chem.* 2014, 53, 872–881

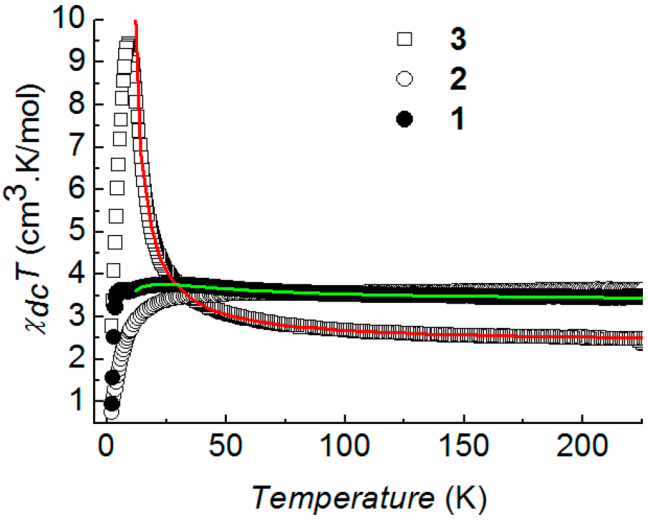

Figure 9. χT product versus temperature of **1**−**3** measured in a dc magnetic field.

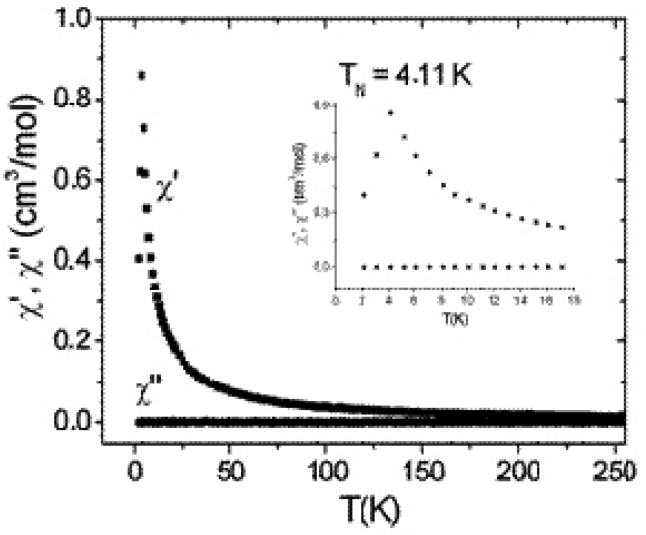

Figure 10. ac field susceptibilities of **1**, χ' and χ'', versus temperature (the inset is a zoom on low temperatures).

Table 3. Characteristic Magnetic Data for 1−3

phase	C (K·emu·mol^{-1})	θ (K)	g	μ_{eff} (μ_B/Ni)
$Ni_3(OH)_2(tp)_2(H_2O)_4$ (**1**)[a]	3.36	+6	2.12	3.0
$Ni_3(OH)_2(tp)_2(H_2O)_2$ (**2**)	3.58	0	2.18	3.1
$Ni_2(OH)_2tp$ (**3**)	2.35	+13	2.17	3.1

[a]tp = $C_8H_4O_4$.

All of the values are consistent with the presence of S = 1 Ni^{II} ions in an octahedral environment.[58] For compound **1**, the χT product increases smoothly from 3.5 K·cm^3·mol^{-1} at 300 K up to a rounded maximum of 3.8 K·cm^3·mol^{-1} at 20 K, indicating a slightly ferromagnetic behavior also denoted by the positive value of θ (Table 3). After a small plateau below 12 K, it drops to zero when cooled to 2 K, which is characteristic of antiferromagnetic ordering.

This ordering was confirmed by ac susceptibility measurements, presented in Figure 10. The temperature variation shows no out-of-phase signal, χ'', whereas a sharp peak of χ' was observed at T_N = 4.1 K.

A 3D antiferromagnetic ordering of the nickel moments agrees with the reversible magnetization versus field variation shown in Figure 11. Above a threshold field of 0.5 T, the magnetization exhibits a metamagnetic transition corresponding to the field-induced alignment of the moments between chains. Thus, the behavior of **1** corresponds to the presence of ferromagnetic nickel(II) chains coupled antiferromagnetically by weak interchain interactions.

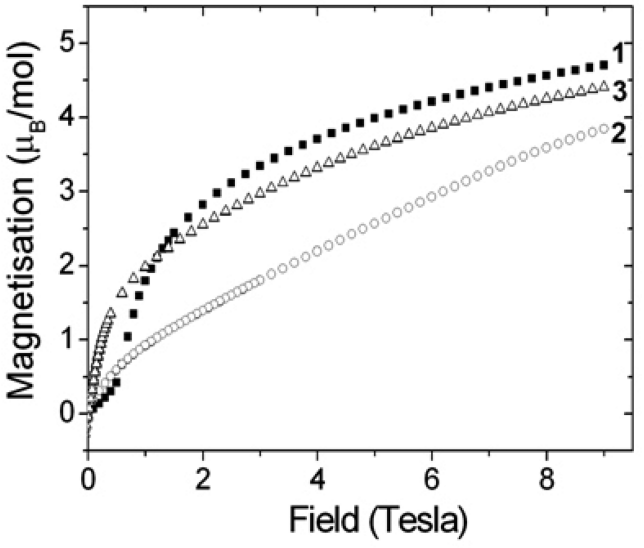

Figure 11. Magnetization versus field in **1**−**3**.

The magnetization is not completely saturated under high field and still increases at 9 T. The high field value of 4.70 μ_B is

Table 4. Magnetic Pathways for 1−3

compound				bond angle (deg)			bond length (Å)
1	Ni1	OH	Ni1	101.3(1)	Ni1	Ni1	3.087(1)
	Ni1	OH	Ni2	125.35(1)	Ni1	Ni2	3.553(1)
	Ni1	OH	Ni2	117.35(1)	Ni2	Ni1	3.488(1)
					Ni2	Ni2	8.007(1)
2	Ni1	OH	Ni1	102.5(3)	Ni1	Ni1	3.232(1)
	Ni1	OH	Ni2	120.4(3)	Ni1	Ni2	3.542(1)
	Ni1	OH	Ni2	121.3(4)	Ni2	Ni1	3.519(1)
	Ni1	OW	Ni1	104.6(6)	Ni2	Ni2	6.278(1)
3	Ni1	OH	Ni1	104.4(3)	Ni1	Ni1	3.318(1)
	Ni1	OH	Ni2	119.1(2)	Ni2	Ni1	3.546(1)
	Ni2	O3	Ni2	98.8(2)	Ni2	Ni2	3.318(1)

dx.doi.org/10.1021/ic402106v | Inorg. Chem. 2014, 53, 872−881

lower than expected for the full alignment of three $S = 1$, $g = 2.12$ Ni ions, i.e., 6.7 μ_B.

Actually, these magnetic features are reminiscent of those found in the thiophenedicarboxylate analogue $Ni_3(OH)_2(TDC)_2(H_2O)_4$ ($TDC^{-} = O_2CC_4H_2SCO_2$), whose structure contains similar nickel chains.[53] In this compound, the magnetic behavior was described as resulting from ferrimagnetic chains coupled antiferromagnetically through the thiophenedicarboxylates. Within the chains, the two Ni1 atoms are coupled ferromagnetically, while the Ni1−Ni2 coupling is antiferromagnetic. This yields a net moment corresponding to two parallel $S = 1$ spins and one in the opposite direction. In the present case with terephthalate ligands, the intermediate M_s value between 2 μ_B (one neat spin moment) and 6.7 μ_B (full alignment of the three moments) suggests that applying a high field counteracts not only the interchain antiferromagnetic coupling but also the Ni1−Ni2 coupling.

To evaluate the couplings, we used the same Heisenberg $S = 1$ chain model as that for the TDC compounds considering the interconnected butterfly motifs shown in Scheme 1.[53]

Scheme 1. Interaction Scheme Considered for the Chain Model Used for Fitting Experimental Data

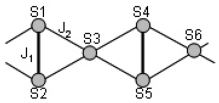

The numerical resolution of the corresponding spin Hamiltonian for six spins yields a very good fit of the experimental data (Figures 9 and S2 in the SI) and led to Ni1−Ni1 interaction $J_1 = +26.6$ K and Ni1−Ni2 interaction $J_2 = -2.8$ K, with $g = 2.1$. These values are like those found for the thiophene analogue. The antiferromagnetic interaction J_2 is really small and an order of magnitude lower than J_1, in accordance with the effect of applying a high field as suggested before. Also, it is consistent with the magnetic structure determined from a combined neutron/powder diffraction and DFT calculations study. The magnetic structure in **1** consists of moments aligned in the *ac* plane with values of 1.7(4) and 1.3(5) μ_B for Ni1 and Ni2, respectively. They form ferrimagnetic chains along the *c* axis, which are combined antiferromagnetically to each other along either the *a* or *b* axis (Figure S1 in the SI).

The χT product of **2** was measured under 0.1 T (see Figure 9). Its overall evolution from room temperature down to 2 K is a regular decrease from 3.5 to 0.75 K·cm^3·mol^{-1}. Some humps are observed in the high-temperature region, around 200 and 50 K, which could correspond to features observed in **1** at different temperatures but are difficult to interpret. Thus, the behavior of **2** is antiferromagnetic. The susceptibility under a static field does not show a maximum ruling out antiferromagnetic long-range ordering. On the contrary, ac susceptibility measurements viewed in Figure 12 show the onset of an out-of-phase signal below $T_C = 3.2$ K, which indicates a magnetic ground state. The real part of χ' exhibits a sharp maximum at T_C. This is consistent with the abrupt increase of the magnetization versus field curve at low field, as seen in Figure 8. Above 0.7 T, the $M(H)$ curve is quasi-linear and the moment at 9 T is weak and comparable to that of compound **1**. Together with the temperature variation of the susceptibility,

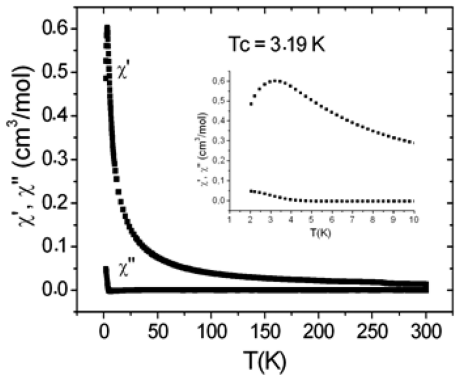

Figure 12. ac susceptibility (zoom in the inset) versus temperature in **2**.

these features are in favor of a weak ferromagnetic state, resulting from a noncollinear (canted) antiferromagnetic ordering below T_C.[58−60]

Models exist for fitting 2D magnetic systems corresponding to hexagonal, triangular, or square-planar spin networks.[61] However, there is no model available for the topology of **2**, which derives from condensation of the mineral chains of **1**. Looking at the structure of the layers in Figure 8, one can expect ferromagnetic Ni1 chains coupled antiferromagnetically with the Ni2 ions, with competition between interactions. Between layers, the interaction is antiferromagnetic. At low temperature, either a single-ion anisotropy of Ni^{II} ions or an antisymmetrical interaction can stabilize a noncollinear ordering.[58]

The dc susceptibility of **3** was measured under a field of 0.5 T. In contrast with **1** and **2**, the χT product increases strongly from 3.7 to 9.43 K·cm^3·mol^{-1} when the temperature decreases between 300 and 6 K, revealing predominant ferromagnetic interactions within the layers, with a positive θ value (Table 1). This divergence of χT suggests a 3D ferromagnetic ordering together with the χ_{ac} measurements reported in Figure 13. A

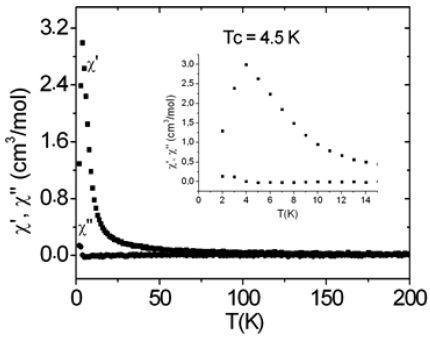

Figure 13. ac susceptibility (zoom in the inset) versus temperature in **3**.

maximum of χ' is observed at $T_C = 4.5$ K. The presence of an out-of-phase signal, χ'', corresponds to a 3D ferromagnetic ordering of the Ni^{2+} moments in accordance with the steep increase of the magnetization curve at 2 K reported in Figure 11. There is no noticeable hysteresis at this temperature, which is very near T_C, implying low anisotropy. The value of the moment 4.4 μ_B/formula unit at 9 T (2.2 μ_B/Ni^{2+}) agrees well with a ferromagnetic state.

As shown in Figure 8, the structure of the layers in **3** can be viewed as a further condensation of the layers in **2**, with some

dx.doi.org/10.1021/ic402106v | Inorg. Chem. 2014, 53, 872−881

tilting of the NiO_6 octahedra and replacement of the water molecules by oxo bridges of hydroxyl groups compared to the initial chains in **1**. The magnetic behavior of **3** is similar to that of the copper derivative $[Cu_2(OH)_2(tp)]$,[35] which orders ferromagnetically below T_C = 4.5 K. As shown in Figure 8, the temperature dependence of the χT product of **3** is well fitted by the exponential function $\chi T = Ce^{E/kT}$. The best-fit values are C = 2.35 K·cm^3·mol^{-1} (the Curie constant) and E/k = 14.23 K (the overall exchange coupling energy). Such exponential variation is characteristic of a 2D Heisenberg system.[60,62,63] Evaluating strictly the in-plane magnetic exchange interactions between the Ni centers leads to consideration of a distorted triangular array of Heisenberg S = 1 spins with interactions corresponding to the different Ni1−Ni1, Ni2−Ni2, and Ni1−Ni2 pathways, which would be very difficult to solve. For comparison with the copper analogue, we thus approximated the system by considering a planar triangular S = 1 spin system with one interaction and one g factor. Within this approximation, the exchange constant between neighboring Ni^{II} ions within the layers was determined from the high-temperature series expansion[61,64,65] for a 2D Heisenberg planar-triangular system:[66]

$$\chi_{pt}(T) = \frac{S(S+1)Ng^2\mu_B^2}{3k_BT}\sum_n a_n x^n \qquad (a)$$

where N, μ_B, and k_B have their usual meanings and $x = J/k_BT$. A good description of the susceptibility, shown in Figure 9, was obtained between 18 and 300 K for S = 1, g = 2.18, and J/k_B = −1.48 K. Although ordering at the same temperature of 4.5 K, the J value is lower than that found for the $S = {}^1/_2$ copper derivative (5.5 K).[35,63] Interestingly, for isotropic spins, the in-plane correlation length ξ is related to the in-plane exchange constant J by the relation[63]

$$\xi^2 = (JS/kT)\exp(4\pi JS^2/kT) \qquad (b)$$

The distance between magnetic layers is quite large for an efficient exchange coupling mechanism. If the interplane coupling consisted only of dipolar interactions, the 3D ordering would depend essentially on the divergence of ξ^2.[67] Figure S3 in the SI shows that ξ^2 is slightly higher for the copper hydroxyterephthalate than for the present nickel compound **3**. Hence, assuming the approximation in the model, one would expect a slightly higher T_C value for the present S = 1 nickel system compared to the copper one. Moreover, the fact that both compounds order at the same temperature and above the temperature at which divergence of ξ^2 is observed suggests a significant through-bond interaction related to spin polarization via the π system of the terephthalate bridges.[68−70]

4. CONCLUSION

The controlled thermal dehydration of compound **1** induces two structural transitions through the sequential loss of two water molecules. Therefore, two new compounds were obtained using this dry route, **2** and **3** at 433 and 483 K, respectively. Compound **2** is of a new structure type. The crystal structure was solved ab initio from PXRD data. Compound **3** was found to be isostructural with $Co_2(OH)_2(tp)$. The structure of **3** was successfully refined from data collected using synchrotron radiation. Compound **2** was obtained by the loss of two water molecules, resulting in coalescence of the nickel chains and the transition from a 1D metallic network to a porous 2D metal framework. Afterward, **2** was transformed to the targeted anhydrous compound **3**, $Ni_2(OH)_2(tp)$, by the loss of the two remaining water molecules accompanied by complex reorganization. These transformations were found to be irreversible and have a direct impact on the magnetic behavior of each phase.

In fact, **1** exhibits a 3D antiferromagnetic ordering below 4.1 K, with metamagnetic behavior beyond a threshold of 0.5 T at 2 K. This behavior results from the presence of ferrimagnetic chains coupled antiferromagnetically to each other. The experimental data were reproduced on the basis of the Heisenberg S = 1 chain model. The result of the fit led to the consideration of chains of ferromagnetic Ni1 dimers coupled with Ni2 through very weak antiferromagnetic interactions. This result is in agreement with the magnetic structure determined by neutron/powder diffraction and was also confirmed by DFT calculations. Compound **2** has ferromagnetic behavior (T_C = 3.2 K), with a noncollinear (canted) arrangement of the magnetic moments. Finally, the anhydrous **3** exhibits 3D ferromagnetic ordering below T_C = 4.5 K. The behavior of **3** shows strong similarities with what is observed in $Cu_2(OH)_2(tp)$,[35] despite their different crystallographic symmetries (the copper-based analogue adopts triclinic symmetry).

In summary, postsynthetic topochemical modifications of the MOFs over a dry route offers an interesting opportunity in terms of the stabilization of new phases not allowed by direct syntheses. In this work, we stabilized a rare anhydrous nickel dicarboxylate compound in two steps using a solid-state route. In the final product, the first neighbors of the Ni ions are only O atoms. Moreover, these modifications are accompanied by significant changes of the magnetic behavior related to the kind of coupling and the magnetic dimensionality of the metal framework.

■ ASSOCIATED CONTENT

Supporting Information

Further details and crystallographic files in CIF format for **2** and **3**. This material is available free of charge via the Internet at http://pubs.acs.org.

■ AUTHOR INFORMATION

Corresponding Author

*E-mail: adel.mesbah@cea.fr.

Present Address

‡(A.M.) ICSM, UMR 5257 CEA/CNRS/UM2/ENSCM, Site de Marcoule, Bât. 426, B.P. 17171, 30207 Bagnols/Cèze Cedex, France.

Notes

The authors declare no competing financial interest.

■ ACKNOWLEDGMENTS

The authors are grateful to Lionel ARANDA (IJL, Nancy, France) for TGA measurements.

■ REFERENCES

(1) Sumida, K.; Rogow, D. L.; Mason, J. A.; McDonald, T. M.; Bloch, E. D.; Herm, Z. R.; Bae, T. H.; Long, J. R. *Chem. Rev.* **2012**, *112*, 724−781.

(2) Suh, M. P.; Park, H. J.; Prasad, T. K.; Lim, D.-W. *Chem. Rev.* **2012**, *112*, 782−835.

(3) Li, J.-R.; Sculley, J.; Zhou, H.-C. *Chem. Rev.* **2012**, *112*, 869−932.

(4) Getman, R. B.; Bae, Y.-S.; Wilmer, C. E.; Snurr, R. Q. *Chem. Rev.* **2012**, *112*, 703−723.

(5) Wu, H.; Gong, Q.; Olson, D. H.; Li, J. *Chem. Rev.* **2012**, *112*, 836−868.
(6) Horcajada, P.; Gref, R.; Baati, T.; Allan, P. K.; Maurin, G.; Couvreur, P.; Ferey, G.; Morris, R. E.; Serre, C. *Chem. Rev.* **2012**, *112*, 1232−1268.
(7) Corma, A.; Garcia, H.; Llabres i Xamena, F. X. *Chem. Rev.* **2010**, *110*, 4606−4655.
(8) Yoon, M.; Srirambalaji, R.; Kim, K. *Chem. Rev.* **2012**, *112*, 1196−1231.
(9) Kreno, L. E.; Leong, K.; Farha, O. K.; Allendorf, M.; Van Duyne, R. P.; Hupp, J. T. *Chem. Rev.* **2012**, *112*, 1105−1125.
(10) Wang, C.; Zhang, T.; Lin, W. *Chem. Rev.* **2012**, *112*, 1084−1104.
(11) Cui, Y.; Yue, Y.; Qian, G.; Chen, B. *Chem. Rev.* **2012**, *112*, 1126−1162.
(12) Mesbah, A.; Jacques, S.; Rocca, E.; François, M.; Steinmetz, J. *Eur. J. Inorg. Chem.* **2011**, 1315−1321.
(13) Mesbah, A.; Juers, C.; François, M.; Rocca, E.; Steinmetz, J. *Z. Kristallogr., Suppl.* **2007**, *2*, 593−598.
(14) Mesbah, A.; Juers, C.; Lacouture, F.; Mathieu, S.; Rocca, E.; François, M.; Steinmetz, J. *Solid State Sci.* **2007**, *9*, 322−328.
(15) Rocca, E.; Caillet, C.; Mesbah, A.; Francois, M.; Steinmetz, J. *Chem. Mater.* **2006**, *18*, 6186−6193.
(16) Sibille, R.; Mazet, T.; Malaman, B.; Francois, M. *Chem.—Eur. J.* **2012**, *18*, 12970−12973.
(17) Jain, P.; Ramachandran, V.; Clark, R. J.; Zhou, H. D.; Toby, B. H.; Dalal, N. S.; Kroto, H. W.; Cheetham, A. K. *J. Am. Chem. Soc.* **2009**, *131*, 13625.
(18) Stroppa, A.; Jain, P.; Barone, P.; Marsman, M.; Perez-Mato, J. M.; Cheetham, A. K.; Kroto, H. W.; Picozzi, S. *Angew. Chem., Int. Ed.* **2011**, *50*, 5847−5850.
(19) Kurmoo, M.; Kumagai, H.; Akita-Tanaka, M.; Inoue, K.; Takagi, S. *Inorg. Chem.* **2006**, *45*, 1627−1637.
(20) Kurmoo, M.; Kumagai, H.; Chapman, K. W.; Kepert, C. J. *Chem. Commun.* **2005**, 3012−3014.
(21) Kurmoo, M.; Kumagai, H.; Hughes, S. M.; Kepert, C. J. *Inorg. Chem.* **2003**, *42*, 6709−6722.
(22) Lee, E. Y.; Suh, M. P. *Angew. Chem., Int. Ed.* **2004**, *43*, 2798−2801.
(23) Xue, D. X.; Zhang, W. X.; Chen, X. M.; Wang, H. Z. *Chem. Commun.* **2008**, 1551−1553.
(24) Zhang, X. M.; Hao, Z. M.; Zhang, W. X.; Chen, X. M. *Angew. Chem., Int. Ed.* **2007**, *46*, 3456−3459.
(25) Serre, C.; Millange, F.; Thouvenot, C.; Nogues, M.; Marsolier, G.; Louer, D.; Férey, G. *J. Am. Chem. Soc.* **2002**, *124*, 13519−13526.
(26) Férey, G.; Serre, C. *Chem. Soc. Rev.* **2009**, *38*, 1380−1399.
(27) Chen, J.; Ohba, M.; Zhao, D.; Kaneko, W.; Kitagawa, S. *Cryst. Growth Des.* **2006**, *6*, 664−668.
(28) Dietzel, P. D. C.; Morita, Y.; Blom, R.; Fjellvag, H. *Angew. Chem., Int. Ed.* **2005**, *44*, 6354−6358.
(29) Volkringer, C.; Loiseau, T.; Guillou, N.; Férey, G. r.; Haouas, M.; Taulelle, F.; Audebrand, N.; Margiolaki, I.; Popov, D.; Burghammer, M.; Riekel, C. *Cryst. Growth Des.* **2009**, *9*, 2927−2936.
(30) Guillou, N.; Livage, C.; Férey, G. *Eur. J. Inorg. Chem.* **2006**, 4963−4978.
(31) Mesbah, A.; Carton, A.; Aranda, L.; Mazet, T.; Porcher, F.; François, M. *J. Solid State Chem.* **2008**, *181*, 3229−3235.
(32) Carton, A.; Mesbah, A.; Mazet, T.; Porcher, F.; François, M. *Solid State Sci.* **2007**, *9*, 465−471.
(33) Huang, Z. L.; Drillon, M.; Masciocchi, N.; Sironi, A.; Zhao, J. T.; Rabu, P.; Panissod, P. *Chem. Mater.* **2000**, *12*, 2805−2812.
(34) Carton, A.; Mesbah, A.; Rabu, P.; François, M. *Z. Kristallogr.* **2007**, *26*, 6.
(35) Abdelouhab, S.; François, M.; Elkaim, E.; Rabu, P. *Solid State Sci.* **2005**, *7*, 227−232.
(36) Barthelet, K.; Marrot, J.; Riou, D.; Férey, G. *Angew. Chem., Int. Ed.* **2002**, *41*, 281−284.
(37) Mesbah, A.; Malaman, B.; Mazet, T.; Sibille, R.; François, M. *CrystEngComm* **2010**, *12*, 3126−3131.
(38) Mesbah, A.; Sibille, R.; Mazet, T.; Malaman, B.; Lebegue, S.; François, M. *J. Mater. Chem.* **2010**, *20*, 9386−9391.
(39) Carton, A.; Mesbah, A.; Perrin, L.; François, M., *Acta Crystallogr., Sect. E: Struct. Rep. Online* **2007**, *63*.
(40) http://www.qdusa.com.
(41) http://www.accelrys.com/products/mstudio/modeling/crystallization/reflex.html.
(42) Neumann, M. A. *J. Appl. Crystallogr.* **2003**, *36*, 356−365.
(43) Favre-Nicolin, V.; Černý, R. FOX: Modular Approach to Crystal Structure Determination from Powder Diffraction. In *Europian Powder Diffrations EPDIC 8*, Uppsala, Sweden, 2004; Materials Science Forum; Andersson, Y., Mittemeijer, E. J., Welzel, U., Eds.; Scientific.Net Materials Science and Engineering: Durnten-Zurich, Switzerland, 2004; pp 35−38.
(44) Rodriguez-Carvajal, J.; Fernandez-Diaz, M. T.; Martinez, J. L. *J. Phys.: Condens. Matter* **1991**, *3*, 3215−3234.
(45) Hohenberg, P.; Kohn, W. *Phys. Rev. B* **1964**, *136*, B864.
(46) Kohn, W.; Sham, L. J. *Phys. Rev.* **1965**, *140*, 1133.
(47) Kresse, G.; Furthmuller, J. *Comput. Mater. Sci.* **1996**, *6*, 15−50.
(48) Kresse, G.; Joubert, D. *Phys. Rev. B* **1999**, *59*, 1758−1775.
(49) Blochl, P. E. *Phys. Rev. B* **1994**, *50*, 17953−17979.
(50) Perdew, J. P.; Burke, K.; Ernzerhof, M. *Phys. Rev. Lett.* **1996**, *77*, 3865−3868.
(51) Liechtenstein, A. I.; Anisimov, V. I.; Zaanen, J. *Phys. Rev. B* **1995**, *52*, R5467−R5470.
(52) Bengone, O.; Alouani, M.; Blöchl, P.; Hugel, J. *Phys. Rev. B* **2000**, *62*, 16392−16401.
(53) Demessence, A.; Mesbah, A.; François, M.; Rogez, G.; Rabu, P. *Eur. J. Inorg. Chem.* **2009**, 3713−3720.
(54) Guillou, N.; Pastre, S.; Livage, C.; Férey, G. *Chem. Commun.* **2002**, 2358−2359.
(55) Konar, S.; Mukherjee, P. S.; Zangrando, E.; Lloret, F.; Chaudhuri, N. R. *Angew. Chem., Int. Ed.* **2002**, *41*, 1561−1563.
(56) Kaduk, J. A. *Acta Crystallogr., Sect. B: Struct. Sci.* **2002**, *58*, 815−822.
(57) Sibille, R.; Mesbah, A.; Mazet, T.; Malaman, B.; Capelli, S.; François, M. *J. Solid State Chem.* **2012**, *186*, 134−141.
(58) Carlin, R. L. *Magnetochemistry*; Springer-Verlang: Berlin, 1986.
(59) Carlin, R. L.; Van Duyneveldt, A. J. *Acc. Chem. Res.* **1980**, *13*, 231−236.
(60) Bauer, E. M.; Bellitto, C.; Righini, G.; Colapietro, M.; Portalone, G.; Drillon, M.; Rabu, P. *Inorg. Chem.* **2008**, *47*, 10945−10952.
(61) Navarro, R. In *Magnetic properties of layered transition metal compounds*; Jongh, L. J. d., Ed.; Kluwer Academic Publishers: Dordrecht, The Netherlands, 1990; pp 105−190.
(62) Souletie, J.; Rabu, P.; Drillon, M. In *Scaling theory applied to low dimensional magnetic systems*; Miller, J. S., Drillon, M., Eds.; Wiley-VCH Verlag GmbH Co. KGaA: Weinheim, Germany, 2005; Vol. *V*.
(63) Suzuki, F.; Shibata, N.; Ishii, C. *J. Phys. Soc. Jpn.* **1994**, *63*, 1539−1547.
(64) Rushbrooke, G. S.; Baker, G. A.; Wood, P. J. In *Wood in Phase Transitions and Critical Phenomena*; Domb, C., Green, M. S., Eds.; Academic Press: London, 1974; Vol. *III*.
(65) Yamaji, K.; Kondo, J. *J. Phys. Soc. Jpn.* **1973**, *35*, 25−32.
(66) [Formule] $x = J/k_BT$, $a_1 = 8$, $a_2 = 49.333332$, $a_3 = 256.0000002$, $a_4 = 1181.48148$, $a_5 = 5054.893818$, $a_6 = 20630.80218$, $a_7 = 81183.44316$, and $a_8 = 307123.1199$.
(67) Drillon, M.; Panissod, P. *J. Magn. Magn. Mater.* **1998**, *188*, 93−99.
(68) Ovchinnikov. *Theor. Chim. Acta* **1978**, *47*, 259.
(69) Rabu, P.; Drillon, M. *Adv. Eng. Mater.* **2003**, *5*, 189−210.
(70) Stroh, C.; Turek, P.; Rabu, P.; Ziessel, R. *Inorg. Chem.* **2001**, *40*, 5334−5342.